Effect of transient pinning on stability of drops sitting on an inclined plane

Viatcheslav Berejnov* and Robert E. Thorne
Physics Department, Cornell University, Ithaca, New York 14853, USA
(Received 23 September 2006; published 11 June 2007)

We report on new instabilities of the quasistatic equilibrium of water drops pinned by a hydrophobic inclined substrate. The contact line of a statically pinned drop exhibits three transitions of partial depinning: depinning of the advancing and receding parts of the contact line and depinning of the entire contact line leading to the drop's translational motion. We find a region of parameters where the classical Macdougall-Ockrent-Frenkel approach fails to estimate the critical volume of the statically pinned inclined drop.

DOI: 10.1103/PhysRevE.75.066308 PACS number(s): 47.55.dr, 47.55.np, 68.08.Bc

I. INTRODUCTION

Dispense a drop on a flat substrate and then tilt it. Depending upon the balance between gravitational and capillary pinning forces, the drop will slide down or stay at rest. Raindrops sticking or sliding on a vehicle windshield provide a familiar example of this drop stability problem, which is of broad practical importance.

In structural genomics, for example, protein crystals are grown by dispensing protein-containing drops onto horizontal glass or plastic substrates. Because protein crystals are extremely fragile, the substrate is then inverted so as to prevent any nucleating crystals from sedimenting onto and adhering to it [1,2]. Crystals in these "hanging drops" instead sediment to the liquid-air interface, where they can be easily extracted without damage. Pinning conditions are important for maintaining the stability and shape of protein solution drops during inversion and handling [3]. Drop instabilities and changes in drop shape affect solvent evaporation rates, protein concentrations, crystal nucleation rates and crystal growth rates—and thus the ultimate quality of the molecular structure determined by x-ray crystallography. Drop shape variations are also a major obstacle to automated optical recognition of the drop's contents, important in high-throughput protein crystallization. More generally, the motion of contact lines is related to motion of elastic manifolds in the presence of disorder [4], including motion of interfaces in porous media and depinning of flux line lattices [5], Wigner crystals, and charge-density waves [6].

The pinning of an inclined drop that prevents its continuous motion is related to the contact angle hysteresis, whose magnitude is usually estimated from the maximum difference between the contact angles θ_a and θ_r at the advancing (downhill) and receding (uphill) edges of the contact line, as shown in Fig. 1. If this maximum difference $\Delta(\cos\theta)_{r,a} = \cos\theta_r - \cos\theta_a$ is nonzero, then drops of volume less than a critical $V_c(\alpha)$ may remain at rest at a given inclination angle α [7,8], although this is a necessary but not sufficient condition for drop stability. The maximum stable drop volume can be estimated by balancing the gravitational force on the drop $F_g = \rho g V \sin(\alpha)$ with the pinning force $F_p \sim \gamma d \Delta(\cos\theta)_{r,a}$.

A simple formula,

$$\Delta(\cos\theta)_{r,a} = AV\sin\alpha, \tag{1}$$

was obtained by Macdougall and Ockrent as a phenomenological explanation of their experiments on inclined drops [8] and independently by Frenkel as a boundary condition of one exactly formulated problem for drop stability on an inclined surface [7]. Here $A = d^{-1}a^{-2}$ is an appropriately scaled material constant, $a = (\gamma/\rho g)^{1/2}$ is the capillary length, and ρ, γ, g, and d are the density, surface tension, gravity, and drop width, respectively.

The Macdougall-Ockrent-Frenkel (MOF) formula Eq. (1) has been widely used to describe the relation between contact angle hysteresis and the equilibrium and criticality of an inclined drop [7–14] from small inclinations and volumes at which the drop deforms but remains static up to the critical inclination or volume at which it begins to slide continuously. The validity of the MOF and related functional forms has been verified in a variety of experiments [8–15], although it has not always correctly predicted the exact volumes of drops pinned at critical conditions. All phenomenological improvements to date have led to the same general form of Eq. (1), with different length factors instead of d.

Despite extensive study, the problem of the stability of a one-component drop on an inclined surface has yet to be addressed in its full richness. Here we examine the equilibrium and criticality of a water drop pinned on a hydrophobic flat glass slide. In particular, we examine a wide range of quasistatic tilting 0°–90° for a moderately hydrophobic surface (~90° contact angle) having a moderate range of contact angle differences ~30°–90°. We show that the MOF criterion, while providing an excellent description for small volumes and inclinations, is not general. Deviations from Eq. (1) at large volumes and angles are associated with transient modes of displacement, whose mechanics have not yet been described. We have clearly resolved partial and global instabilities of the contact line. Three coexistence curves corresponding to partial depinning of the advancing and receding parts of the contact line and to depinning and continuous motion of the entire contact line mark those instabilities unambiguously. The transient displacements of the advancing and receding parts of the contact line have different scalings. We find a region of parameter space where the difference

*Also at Institute for Integrated Energy Systems, University of Victoria, P.O. Box 3055, Victoria, BC V8W 3P6, Canada. Electronic address: berejnov@uvic.ca

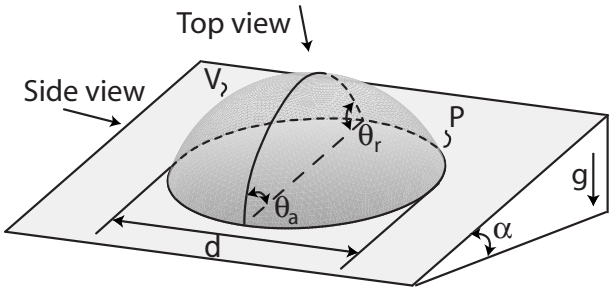

FIG. 1. A drop on an inclined surface, characterized by the drop volume V and diameter d, the contact line perimeter p, the advancing and receding contact angles θ_a and θ_r, and the substrate inclination angle α. Observations from above can determine the shape and position of the contact line, while observations from the side can determine the contact angles.

between the drop's maximum and minimum contact angles cannot reliably be used to predict the maximum pinning strength and the onset of drop sliding.

II. CONTACT LINE STABILITY AND DEPINNING FOR AN INCLINED DROP

A drop's contact line, between its initially static pinned state and its steady sliding motion, may exhibit a continuous series of intermediate states. This fact has been previously noted [10,11,13,16], but its effect on the stability of an inclined drop has not been fully appreciated.

After being dispensed on a homogeneous, flat, horizontal substrate, a drop will have a circular contact line. As the substrate angle α is slowly stepped upward, a drop of volume V eventually becomes unstable and slides continuously down the substrate. At a smaller angle, the drop's contact line may become locally unstable, and undergo local displacements that change the contact line's shape but that do not produce continuous motion. Although these critical angles for the onset of global and local instability are in general different, for some experimental conditions they may be only weakly distinguishable in measurements. In this case, the transient pinning of the contact line does not affect drop criticality and may be neglected. The drop equilibrium and criticality may then be described in terms of a simple energetic balance, as in the MOF formula, between the potential and capillary energies of the inclined drop.

When the global and local equilibriums are well separated, the contact line can be displaced over the substrate while simultaneously maintaining its stability against continuous sliding. In this case, because the contact line configuration corresponding to the global equilibrium is unknown, the simple energetic balance describing the drop stability criterion should be reconsidered.

Several attempts to analytically describe the shape, reconfigurations, and criticality of the contact line for an inclined drop have been reported. In 1948, using a variational technique to analyze the drop shape for small inclinations, Frenkel [7] explicitly showed for a two-dimensional (2D) inclined drop that equilibrium conditions and translational drop instability lead to the MOF criteria Eq. (1). Popova [17] extended the variational technique to a 3D drop at small inclination. She analytically calculated the equilibrium drop shape, contact line shape, and the contact angle as a function of position along the contact line. Carre and Shanahan [18] followed a similar approach to calculate the pinning force, and obtained a criticality equation similar to the MOF criterion Eq. (1). Dussan [19], stimulated by earlier experiments [10,11], studied criticality of 3D inclined drops with an initially elliptical rather than circular contact line. Using the equations of continuous fluid dynamics, she found an equation for the equilibrium states of the inclined drop at small hysteresis, which can be used to obtain the drop's critical conditions. Popov [20] used a variational analysis to examine the equilibrium and criticality of a weakly perturbed hemispherical drop at large inclinations. His solution describes well only the stability of small drops inclined near $\alpha=90°$.

In all the above studies [7,17–20], the contact line shape was either arbitrarily chosen or else determined from the minimum of some free energy.

Furthermore, in all cases the chosen contact line shape was assumed to be maintained up to and including the critical point for the onset of instability and drop sliding. Consequently, these approaches ignored the transitional behavior of the contact line prior to global criticality.

In addition to these analytic attempts, two numerical studies [21,22] have explored freely displacing contact lines. Dimitrakopoulos and Higdon [21] reported transient contact line behavior similar to that observed here. However, the implementation of pinning in the numerical algorithm, which leads to contact profiles resembling those found in experiment, was not derived from fundamental considerations, and their y-constrained boundary conditions need further clarification and justification. Iliev [22] used a two-parameter phenomenological model to describe the pinning. However, the connection between those parameters and experiment is unclear, and drop deformations and criticality curves were not calculated, making comparison with the present results difficult.

III. MATERIAL AND EXPERIMENTAL METHODS

Distilled and deionized water purified by a NANOpure II system (Barnstead, Boston, MA) was dispensed onto siliconized flat glass slides with diameter of 22 mm (HR3-231, Hampton Research, Laguna Niguel, CA). On a freshly unpackaged slide, a 40-μl water drop formed a reproducible contact angle of 90°–92°. To determine drop stability on a given slide, a drop was manually dispensed onto a horizontal slide using a 100-μl micropipette (Pipetman Co., France). The slide was then slowly rotated in 2°–4° steps on a home-built rotation stage. The time interval between rotations was roughly 1 min, long enough to allow transient shape relaxations to dissipate. A 640×480-pixel resolution digital camera (Cohu, San Diego, CA) with a telecentric 55-mm objective (Computar, Japan) was mounted on the rotation stage, and aimed perpendicular to plane of the slide (corresponding to the "top view" in Fig. 1). Image recording at six frames per second began immediately after each stage rotation was completed and continued throughout the entire relaxation pe-

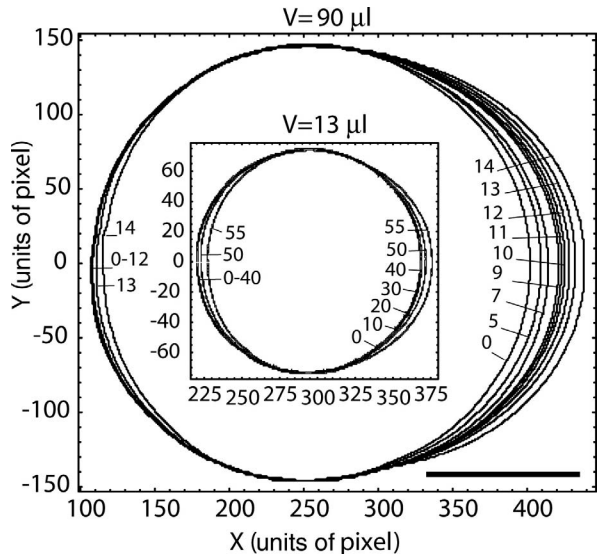

FIG. 2. Views normal to the substrate plane of the static contact lines for two drops, achieved as the substrate inclination is increased. The coordinates are in pixels, with the same image magnification for both drops, and the scale bar is 2.6 mm long. The numbers on each contact line indicate the substrate inclination α in degrees.

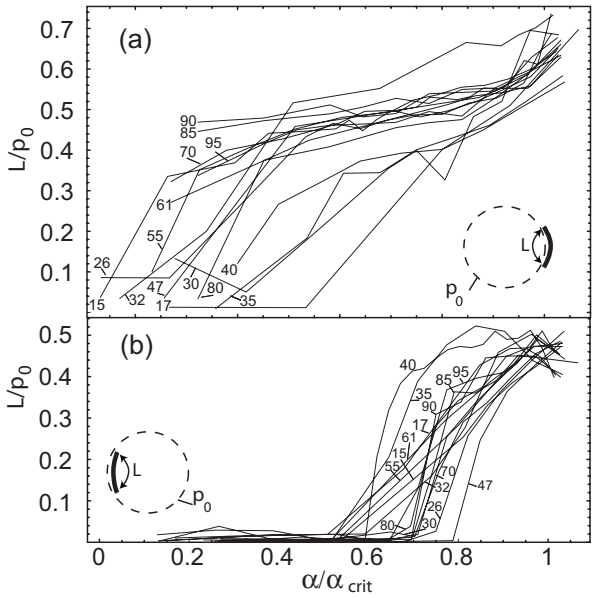

FIG. 3. Total displaced length of the contact line L at (a) the advancing and (b) the receding edges as a function of drop inclination angle α. The initial drop perimeter at $\alpha=0°$ is p_0, and at α_{crit} the contact line can no longer find a static configuration and begins to slide continuously. The numbers on each curve denote the drop volumes in μl.

riod. A custom image recognition program was written and implemented in LABVIEW to process each image to extract the contact line. Figure 2 shows examples of contact line profiles at different tilt angles determined in this way.

The apparent contact angles at the advancing and receding contact lines were measured from the drop "side view" in Fig. 1 using an independent horizontal goniometer. Dispensed drop volumes were accurate to 0.1–0.5 %, and tilt and contact angle measurements were accurate to 1°–2°. Measured velocities U of contact line motion during the transient displacements were <0.1 mm/s. Using water's dynamic viscosity $\eta\sim 0.01$ g/(cm s) and surface tension $\gamma\sim 70$ dyn/cm yields an upper bound $<10^{-6}$ for the capillary number $\mathrm{Ca}=U\eta/\gamma$. Thus all dynamic effects during contact line rearrangement can be neglected.

On a horizontal, homogeneous flat surface, a drop's minimum free-energy configuration has a circular contact line. In practice, the actual contact line shape depends on the initial contact conditions formed while the drop is dispensed. We found that the subsequent contact line displacements depend upon the contact line's initial shape and on the initial contact angles along it. Consequently, we carefully prepared and selected drops with initially circular contact lines.

IV. RESULTS

Figure 2 shows typical results for the contact line position recorded at different tilt angles, for two drops with volumes of 13 and 90 μl, respectively. As the substrate is tilted, the contact line initially remains pinned in its original circular configuration. Beyond a first critical tilt angle α_a, the advancing portion of the contact line becomes locally unstable and displaces in an attempt to find a new equilibrium, eventually reaching a new static configuration. Beyond a second, larger critical angle α_r, the receding part of the contact line becomes locally unstable and displaces, but the drop again finds a new static configuration. Beyond a third critical angle of inclination α_{crit}, the drop becomes unstable and slides continuously.

The difference in the behavior of the advancing and receding contact lines implies that pinning along the contact line is not homogeneous. This conclusion is consistent with previous calculations and measurements [18,23–25] of the contact angles along a contact line's circumference.

Figure 3 examines how the displaced length L of the static contact line evolves with respect to the critical parameters α and V. The total displaced length L of the contact line at the advancing and receding edges following a tilt increment to angle α can be determined by subtracting images acquired at $\alpha=0°$ from those at that angle α. For small α such that the contact line remains circular, the resulting difference images still show some displaced pixels that are randomly distributed over the contact line, arising from noise and other measurement errors. In Fig. 3(a) and especially Fig. 3(b), this noise produces the small-α deviations from $L/p_0=0$. At larger α (beyond α_a or α_r), the advancing or receding part of the contact line begins to displace (Fig. 3 insets), and the difference image shows a chain of connected pixels. This chain grows on further inclination to form a displacing front of length L. Figure 3 plots L/p_0 vs α/α_{crit}, where p_0 is the unperturbed drop perimeter (at $\alpha=0°$) and α_{crit} corresponds to the onset of drop instability and continuous translational motion.

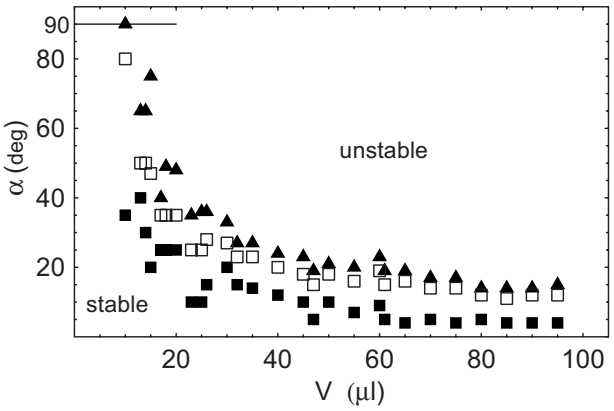

FIG. 4. Contact line transitions as a function of substrate inclination angle α and drop volume V. Symbols denote ■: onset of quasistatic displacements of the advancing contact line; □: onset of quasistatic displacements of the receding part; and ▲: onset of continuous motion of the whole contact line.

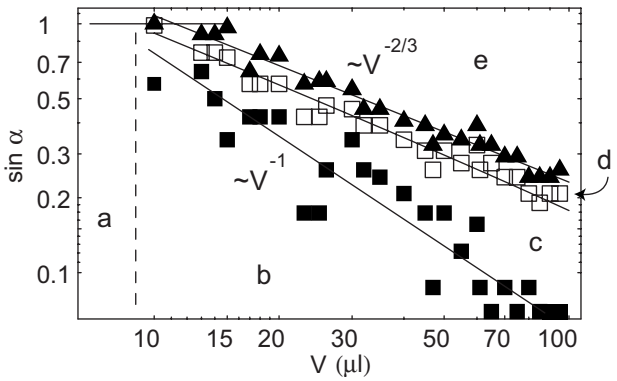

FIG. 5. Log-log representation of Fig. 4. The letters denote zones where (a) the contact line is absolutely stable against any inclination, (b) the contact line is stable up to a maximum inclination $<90°$, (c) the contact line locally displaces to a new static configuration, (d) the contact line globally displaces to a new static configuration, (e) the contact line is unstable and moves continuously.

Figure 3 visualizes unambiguously the fact noted previously [10,11,13,16] that the advancing contact line may displace at a lower inclination angle than the receding contact line. Although there is considerable scatter in the data, there is still remarkable consistency in behavior over the factor-of-10 volume range examined. The advancing contact line begins moving at a small $\alpha/\alpha_{crit}<0.2$ and the displaced length L/p_0 grows monotonically, reaching a consistent value of $\sim 0.6\pm 0.1$ just before α_{crit}. In contrast, the receding contact line remains pinned until $\alpha/\alpha_{crit}>0.6-0.8$, and then steeply increases to $L/p_0\sim 0.5$ at α_{crit}. Note that, because the drop becomes distended, the total contact line length near α_{crit} exceeds its initial length p_0.

Figure 4 presents a subset of the data in Fig. 2, plotted in the space of critical parameters V and α. The solid ■ and open □ squares indicate the onset of local instability at the advancing and receding parts of the contact line, respectively, and the solid triangles ▲ indicate the onset of continuous drop motion.

The curves ■ and ▲ bound a zone of metastability of the pinned contact line, where an appropriate disturbance (e.g., tilt or vibration) can lead to depinning and either reconfiguration to a new static configuration or to continuous sliding. This metastability may explain uncertainties in previous measurements of critical volumes of inclined drops [12,14,15,26,27].

A log-log scaling of these data is presented in Fig. 5, and clarifies the observed differences in the transient displacements of the contact lines. Between absolute stability [zone (a)]—where the initial circular contact line is maintained at all inclinations—and continuous motion [zone (e)], the contact line passes through three transitions: instability of the advancing line at $\alpha_a(V)$ (Fig. 4, curve ■), instability of the receding line at $\alpha_r(V)$ (Fig. 4, curve □), and finally, instability at $\alpha_{crit}(V)$ leading to continuous translational motion of the entire contact line (curve ▲). Figure 5 also clearly shows that there are five zones of behavior in the space (V,α) in which the contact line loses its stability. In addition to zones (a) and (e), in zone (b) the contact line is stable only up to a maximum inclination $<90°$. In zone (c), between the ■ and □ transition curves, the contact line shows partial instability at its advancing edge. In zone (d) both the advancing and receding portions participate in quasistatic displacements, but the drop still remains at rest.

Scatter in the data of Figs. 4 and 5 is due to variations in pinning properties from glass slide to glass slide. The measurement uncertainties in α and $\sin(\alpha)$ are comparable to the size of the symbols.

Fits to the data in Fig. 5 indicate that there is not a unique scaling for the three transitions. No contact line motion is observed in region (a) at inclinations up to and including 90°. Consequently, all three fits should intersect $\sin(\alpha)=1$ at or to the right of the dotted line [assuming that the $\sin(\alpha)-V$ relation is a simple power law]. The receding contact line transition and the transition to continuous sliding have the same volume scaling $V^{-0.75}\sim V^{-2/3}$. However, the best fit to the advancing transition data scales as $V^{-1.06}\sim V^{-1}$. If a $V^{-2/3}$ scaling is assumed, the $\sin(\alpha)=1$ intercept lies well to the left in region (a), even if the data for $\sin(\alpha)<0.15$ is excluded. This suggests that the advancing instability is controlled by disturbances that do not scale like the drop size. The length factor d in the MOF formula for the advancing part of the contact line should thus be replaced by some new scaling δ, which is independent of the drop size and may be related to the length scale of local perturbations.

Figure 6 shows the measured apparent advancing and receding contact angles vs inclination angle, for drop volumes ranging over a factor of 8. The measurements were performed for each particular drop volume at inclinations below α_{crit}, for which the contact line reached a static configuration after each inclination increment. Solid guide lines denote the stable regions [(a) and (b) in Fig. 5], and dashed lines indicate zones of partial instability at the advancing and receding edges [(c) and (d) in Fig. 5]. The drop contact line traverses

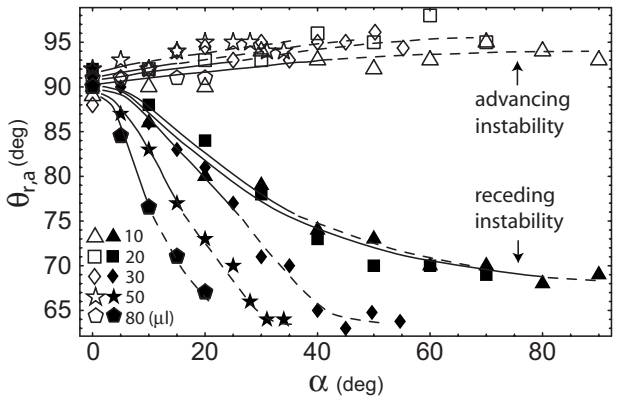

FIG. 6. Apparent values of the advancing contact angle θ_a (open symbols) and receding contact angle θ_r (closed symbols) vs inclination α, for five different volumes V. The lines are guides to the eye, and are comprised of a solid segment where the contact line remains pinned in its initial $\alpha=0°$ configuration [regions (a) and (b) in Fig. 5] and dashed segment where the contact line undergoes local displacements [regions (c) and (d) in Fig. 5]. The contact line as a whole remains in static equilibrium until the end of the dashed line, and slides continuously beyond it (the ▲ line in Fig. 5).

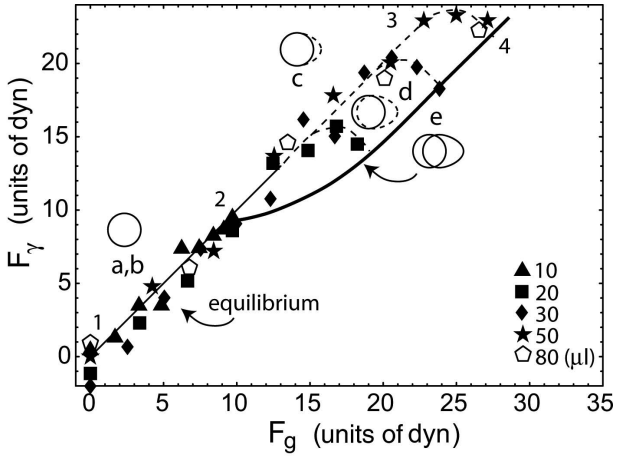

FIG. 7. Equilibrium and criticality of an inclined drop. Symbols indicate the evolution of drops from static pinning to continuous sliding, for five different volumes. The solid line 1-2 is a fit to the MOF formula [Eq. (1)], the dashed lines show how the data deviate from this fit, and the solid curve 2-4 indicates instability of the contact line (the ▲ line in Fig. 5). The letters and insets represent the same regions plotted in Fig. 5 and different kinds of displacement of the contact line, respectively. For definitions of F_γ and F_g see the text.

the stable zones (a) and (b), passes the advancing and receding displacement transitions and the zones of partial instability (c) and (d), and eventually reaches the globally unstable zone (e). These data deviate significantly from those presented in Ref. [28], where a hydrophobic substrate was also used. In particular, while the advancing angle in Fig. 6 is nearly independent of drop volume, the receding angle depends strongly upon drop volume.

Figure 6 raises another interesting question, touched on in [29]: which values of the advancing and receding contact angles θ_a and θ_r for a given drop volume do we have to choose for an adequate description of contact line pinning and stability? According to Figs. 5 and 6, the advancing and receding angles often lie in different zones of stability in Fig. 5. In particular, the last absolutely stable value of θ_r (indicated in Fig. 6 by the points at which the solid curves connect to the dashed ones) do not have corresponding absolutely stable values of θ_a.

The existence of metastable zones (c) and (d) is not anticipated by the simple force balance that leads to Eq. (1), and complicates the comparison of Eq. (1) to experiment. More detailed models that have led to relations of the MOF form have assumed that the contact line remains in its $\alpha=0°$ configuration until the drop as a whole depins and slides. The contact angles θ_a and θ_r in Eq. (1) are then those for the inclination α at the onset of global instability, corresponding to the last points on the dashed curves in Fig. 6, and to the ▲-transition curve in Figs. 4 and 5. But since the contact line in fact exhibits local instabilities before the onset of global instability, it is not obvious that this traditional choice of contact angles is correct. In the absence of a clear alternative, we will use this choice to compare Eq. (1) with experiment.

Figure 7 compares the MOF equation for the equilibrium and stability of inclined drops with our experiments. Using the perimeters p from images similar to those presented in Fig. 2 and the traditional choice for the contact angles θ_a and θ_r to quantify the contact angle difference, we may rescale the data of Figs. 4 and 6 using $F_\gamma=\gamma(\cos\theta_r-\cos\theta_a)p/2\pi$ and $F_g=V\rho g\sin\alpha$ such that the MOF fit of Eq. (1) appears as a straight line. At small values of the scaled variables, the data are in fact linear, and a fit gives $\gamma=72$ dyn/cm, consistent with the accepted value for water at $T=22$ C of 72.5 dyn/cm.

The portion 1-2 of the solid line corresponds to regions (a) and (b) in Fig. 5, where the contact line does not displace from its initial $\alpha=0$ configuration. In this range of parameters, Eq. (1) provides an excellent fit to the data, as has been observed in many previous studies [8,10–14].

For larger drop volumes, Eq. (1) continues to provide an excellent fit, suggesting that the quasistatic contact line displacements do not appreciably affect the overall drop shape and drop pinning. The line 2-3 corresponds to the region (c) in Fig. 5 where the advancing part of the contact line is not stable and exhibits quasistatic displacements.

The points at largest F_g—on the "hooks" of the dashed curves in Fig. 7—represent the last stable contact line configurations, corresponding to the ▲ line in Fig. 5. The zone between curves 2-3 and 2-4 corresponds to the (d) region of Fig. 5. According to Fig. 5, in this zone both the advancing and receding contact lines are locally unstable and undergo quasistatic displacements. In this zone there are clear and large deviations from the MOF fit. The last stable points form the criticality curve roughly presented by curve 2–4.

V. CONCLUSIONS

The present experiments show that the standard picture of instability of inclined drops, as assumed in previous analyti-

cal treatments, is oversimplified. In particular, the assumption that the contact line remains unchanged with inclination until it begins to slide does not adequately describe the actual depinning. By quantifying the metastable displacements that precede global depinning, the present results provide a basis for a more complete treatment of inclined drop stability.

ACKNOWLEDGMENTS

This work was supported by the NIH Grant No. R01 GM65981-01. We thank C. W. Extrand for helpful and stimulating email discussion and P. Dimitrakopoulos and M. H. Murray for critical reading of our manuscript.

[1] Hampton Research, in *Crystallization Research Tools* (Hampton Research, Laguna Niguel, CA, 2003), Vol. 13.
[2] A. McPherson, *Crystallization of Biological Macromolecules* (Cold Spring Harbor Laboratory Press, New York, 1999).
[3] V. Berejnov and R. E. Thorne, Acta Crystallogr., Sect. D: Biol. Crystallogr. **61**, 1563 (2005).
[4] D. S. Fisher, Phys. Rep. **301**, 113 (1998).
[5] G. Blatter *et al.*, Rev. Mod. Phys. **66**, 1125 (1994).
[6] R. E. Thorne, Phys. Today **49** (5), 42 (1996).
[7] Y. I. Frenkel, Zh. Eksp. Teor. Fiz. **18**, 659 (1948). This work, to date available only in Russian, has not been adequately appreciated, so we have made a translation available at http://xxx.lanl.gov/abs/physics/0503051
[8] G. Macdougall and C. Ockrent, Proc. R. Soc. London, Ser. A **180**, 0151 (1942).
[9] Y. B. Aron and Y. I. Frenkel, Zh. Eksp. Teor. Fiz. **19**, 807 (1949).
[10] J. J. Bikerman, J. Colloid Sci. **5**, 349 (1950).
[11] C. G. Furmidge, J. Colloid Sci. **17**, 309 (1962).
[12] K. Kawasaki, J. Colloid Sci. **15**, 402 (1960).
[13] C. W. Extrand and Y. Kumagai, J. Colloid Interface Sci. **170**, 515 (1995).
[14] P. Roura and J. Fort, Phys. Rev. E **64**, 011601 (2001).
[15] N. Le Grand, A. Daerr, and L. Limat, J. Fluid Mech. **541**, 293 (2005).
[16] C. W. Extrand and A. N. Gent, J. Colloid Interface Sci. **138**, 431 (1990).
[17] L. N. Popova, Fluid Dyn. **18**, 634 (1983).
[18] A. Carre and M. E. R. Shanahan, J. Adhes. **49**, 177 (1995).
[19] E. B. Dussan, J. Fluid Mech. **151**, 1 (1985).
[20] V. G. Popov, High Temp. **28**, 731 (1990).
[21] P. Dimitrakopoulos and J. J. L. Higdon, J. Fluid Mech. **395**, 181 (1999).
[22] S. D. Iliev, J. Colloid Interface Sci. **194**, 287 (1997).
[23] R. A. Brown, F. M. Orr, Jr., and L. E. Scriven, J. Colloid Interface Sci. **73**, 76 (1980).
[24] A. I. ElSherbini and A. M. Jacobi, J. Colloid Interface Sci. **273**, 556 (2004).
[25] R. Finn, *Equilibrium Capillary Surfaces* (Springer-Verlag, New York, 1986).
[26] D. Quéré, M. J. Azzopardi, and L. Delattre, Langmuir **14**, 2213 (1998).
[27] H. V. Nguyen, S. Padmanabhan, W. J. Desisto, and A. Bose, J. Colloid Interface Sci. **115**, 410 (1987).
[28] E. Wolfram and R. Faust, in *Wetting, Spreading and Adhesion*, edited by J. F. Padday (Academic Press, New York, 1978), pp. 213–222.
[29] B. Krasovitski and A. Marmur, Langmuir **21**, 3881 (2005).